MARTIN MARIETTA ENERGY SYSTEMS LIBRARIES

3 4456 0266329 5

ORNL/TM-10382

ornl

OAK RIDGE
NATIONAL
LABORATORY

MARTIN MARIETTA

Volt-Second Consumption in Tokamaks with Sawtooth Activity

W. A. Houlberg

OAK RIDGE NATIONAL LABORATORY
CENTRAL RESEARCH LIBRARY
CIRCULATION SECTION
4500N ROOM 175
LIBRARY LOAN COPY
DO NOT TRANSFER TO ANOTHER PERSON
If you wish someone else to see this report, send in name with report and the library will arrange a loan.

OPERATED BY
MARTIN MARIETTA ENERGY SYSTEMS, INC.
FOR THE UNITED STATES
DEPARTMENT OF ENERGY

Printed in the United States of America. Available from
National Technical Information Service
U.S. Department of Commerce
5285 Port Royal Road, Springfield, Virginia 22161
NTIS price codes—Printed Copy: A03; Microfiche A01

This report was prepared as an account of work sponsored by an agency of the United States Government. Neither the United States Government nor any agency thereof, nor any of their employees, makes any warranty, express or implied, or assumes any legal liability or responsibility for the accuracy, completeness, or usefulness of any information, apparatus, product, or process disclosed, or represents that its use would not infringe privately owned rights. Reference herein to any specific commercial product, process, or service by trade name, trademark, manufacturer, or otherwise, does not necessarily constitute or imply its endorsement, recommendation, or favoring by the United States Government or any agency thereof. The views and opinions of authors expressed herein do not necessarily state or reflect those of the United States Government or any agency thereof.

ORNL/TM-10382
Dist. Category UC-20 g

Fusion Energy Division

VOLT-SECOND CONSUMPTION IN TOKAMAKS WITH SAWTOOTH ACTIVITY

W. A. Houlberg

DATE PUBLISHED — July 1, 1987

Prepared by the
OAK RIDGE NATIONAL LABORATORY
Oak Ridge, Tennessee 37831
operated by
MARTIN MARIETTA ENERGY SYSTEMS, INC.
for the
U.S. DEPARTMENT OF ENERGY
under contract DE-AC05-84OR21400

CONTENTS

ACKNOWLEDGMENT v

ABSTRACT vii

1 INTRODUCTION 1

2 FLUX EQUATIONS FROM FARADAY'S LAW 2

3 FLUX EQUATIONS FROM POYNTING'S THEOREM 3

4 FLUX AND ENERGY EFFECTS OF MHD ACTIVITY 5

5 KADOMTSEV'S MODEL FOR FLUX REDISTRIBUTION 7

6 APPLICATION TO CIT 9

7 SUMMARY 17

REFERENCES 21

MARTIN MARIETTA ENERGY SYSTEMS LIBRARIES

3 4456 0266329 5

ACKNOWLEDGMENT

The author wishes to acknowledge very helpful discussions with his colleagues. This work has benefitted from many fruitful discussions with S. C. Jardin on comparisons with TSC calculations and with M. G. Bell, B. A. Carreras, S. Ejima, R. J. Hawryluk, S. P. Hirshman, and P. R. Thomas on formulation of the volt-second problem and interpretation of the various terms.

ABSTRACT

The effects of sawtooth activity on the poloidal magnetic flux and energy balances in tokamak plasmas on a diffusive timescale are evaluated through the application of conservation principles to Maxwell's equations. Poloidal magnetic flux (volt-second) consumption can be partitioned into internal and dissipative components by two methods: the 'axial method' based on a magnetic flux balance and the 'Poynting method' based on a magnetic energy balance. Both require additional terms that specifically account for the poloidal flux and magnetic energy changes during magnetic reconnection derived from analysis on a magnetohydrodynamic (MHD) timescale. In experimental analyses these terms are absorbed in the inferred resistive dissipation, while in predictive analyses they must be evaluated directly. The dissipation of poloidal flux by sawtooth activity can exceed the normal resistive dissipation when the axial method of accounting is used.

1 INTRODUCTION

Analysis of the poloidal magnetic field system is an important part of the design of any large tokamak; accuracy is required to establish the size of the Ohmic heating transformer, which in turn has a direct influence on the size and pulse length of the device. Since the magnetic flux (webers, more commonly called volt-seconds) consumption during the flat-top portion of a typical pulsed tokamak plasma is small compared to the startup requirements, relatively small errors in the analysis can translate into a large variation in the flat-top pulse length at full operating parameters. This is particularly true of Compact Ignition Tokamak (CIT) designs that use high toroidal and poloidal magnetic fields to approach ignition and have relatively short flat-top phases.

The largest uncertainty is in obtaining the internal flux content and the rate of dissipation of that flux. The toroidal current profile and the means by which it evolves are at the heart of this analysis. Classical or neoclassical electrical resistivity is usually assumed as the means for current penetration and flux dissipation. However, internal MHD instabilities, such as sawtooth and double-tearing modes, also play a role in the evolution of the current distribution. So the question of how these rapid, periodic flux redistribution processes affect volt-second consumption needs to be addressed in both diagnostic and predictive analyses.

Two methods have been employed in analyzing the volt-second consumption in tokamak experiments: the 'axial method' based on the integral form of Faraday's law [1] and the 'Poynting method' based on the integral form of Poynting's theorem [2]. The total volt-seconds is measured in experiments, but the relative assignment of dissipative and internal contributions differs for the two methods as shown by Ejima et al. [2]. Derivations of the relevant equations and definitions of inductances are given in Sections 2 and 3. With either method, the dissipative component can be further broken down into a resistive diffusion component and a magnetic reconnection component. A set of integral constraints imposed by Faraday's and Ampère's laws is developed in Section 4 to carry the effects of a restructured magnetic field through the magnetic flux and energy balances.

An empirical description for flux redistribution due to sawtooth activity, common in transport simulation, is given in Section 5 and applied in Section 6 to investigate the possible effects of sawtooth activity on volt-second consumption in a CIT. Predictive analysis, in its most developed form, requires a set of circuit equations coupling the external coils, the eddy currents in the structure, and a model for evolution of the current distribution in the plasma with MHD equilibrium constraints [3]. The analysis is truncated at the plasma boundary; only the relationship between the loop voltage at the plasma edge, $V_\phi(a,t)$, and the plasma internal parameters is considered. The total flux required in the core of the primary is obtained by adding the external flux to the time integral of the loop voltage [4].

2 FLUX EQUATIONS FROM FARADAY'S LAW

The magnetic flux balance is obtained from integration of Faraday's law,

$$-\dot{\vec{B}} = \nabla \times \vec{E} \tag{1}$$

over a toroidal strip, $\vec{S}_\theta$, bounded by the magnetic axis and the plasma edge (labelled $\rho = 0$ and $\rho = a$ respectively, where ρ is a flux surface label). This yields

$$\begin{aligned} -\int \dot{\vec{B}} \cdot d\vec{S}_\theta &= \int (\nabla \times \vec{E}) \cdot d\vec{S}_\theta \\ &= \oint_0 \vec{E} \cdot d\vec{l}_\phi - \oint_a \vec{E} \cdot d\vec{l}_\phi \\ &= V_\phi(0,t) - V_\phi(a,t) \end{aligned} \tag{2}$$

where the ϕ and θ subscripts designate toroidal and poloidal directions, respectively. The right side represents the difference between edge and axial loop voltages, and the left side consists of the time rate of change of the internal poloidal magnetic flux used in MHD analysis, denoted here as Ψ^F_{int} (where the superscript F refers to Faraday's law), plus a term due to a change in internal geometry,

$$\begin{aligned} \int \dot{\vec{B}} \cdot d\vec{S}_\theta &= \frac{d}{dt} \int \vec{B} \cdot d\vec{S}_\theta - \int \vec{B} \cdot d\dot{\vec{S}}_\theta \\ &= \dot{\Psi}^F_{\text{int}}(t) - \int \vec{B} \cdot d\dot{\vec{S}}_\theta \end{aligned} \tag{3}$$

Integration over time then yields the axial form of the volt-second balance at the plasma surface:

$$\Psi^F_a(t) \equiv \int V_\phi(a,t)\, dt = \int dt \left[V_\phi(0,t) + \dot{\Psi}^F_{\text{int}}(t) - \int \vec{B} \cdot d\dot{\vec{S}}_\theta \right] \tag{4}$$

The last term can be ignored except when the plasma boundary changes (e.g., during compression) or when the shift of the magnetic axis changes rapidly (e.g., during auxiliary heating when the β_θ increase is large); it is primarily governed by the vertical field. (In the sawtooth flux redistribution model discussed later, the geometry is kept fixed and this term identically vanishes; it appears, however, when the next MHD equilibrium is calculated.) Dropping this term gives [1]:

$$\Psi^F_a(t) \approx \int dt \left[V_\phi(0,t) + \dot{\Psi}^F_{\text{int}}(t) \right] \tag{5}$$

The time integral has not been carried through the terms on the right so that the contributions from different timescale processes can be evaluated more readily in Section 4.

An internal inductance, L^F_{int}, or internal inductivity, h_i, relating Ψ^F_{int} and toroidal current in the plasma, I_ϕ, can be defined as:

$$L^F_{\text{int}}(t) \equiv \frac{\mu_0 R_0 h_i(t)}{2} \equiv \frac{\Psi^F_{\text{int}}(t)}{I_\phi(t)} \tag{6}$$

This should not be confused with the internal inductance defined from the magnetic energy content in Section 3.

In a similar fashion, Faraday's law can be integrated over the poloidal cross section to yield the toroidal flux balance:

$$\int V_\theta(a,t)\,dt = \int dt\left[-\dot{\Phi}_a(t) + \int \vec{B}\cdot d\dot{\vec{S}}_\phi\right] \tag{7}$$

where Φ_a is the internal toroidal flux. Equation (7) shows that a poloidal voltage is induced at the plasma edge when the toroidal flux changes within a fixed volume. In the absence of changes in the toroidal field coil current, toroidal flux changes are produced by changes in plasma paramagnetism or diamagnetism.

3 FLUX EQUATIONS FROM POYNTING'S THEOREM

The poloidal magnetic energy balance comes from integration of Poynting's theorem (the scalar product of Faraday's law with $\vec{B}_\theta$ plus the scalar product of Ampère's law with $\vec{E}_\phi$),

$$-\frac{\partial}{\partial t}\left(\frac{B_\theta^2}{2\mu_0}\right) - E_\phi J_\phi = \frac{1}{\mu_0}\nabla\cdot(\vec{E}_\phi\times\vec{B}_\theta) \tag{8}$$

over the entire plasma volume V:

$$\begin{aligned}
-\int\frac{\partial}{\partial t}\left(\frac{B_\theta^2}{2\mu_0}\right)dV - \int E_\phi J_\phi dV &= \frac{1}{\mu_0}\int\nabla\cdot(\vec{E}_\phi\times\vec{B}_\theta)\,dV \\
&= \frac{1}{\mu_0}\oint(\vec{E}_\phi\times\vec{B}_\theta)\cdot d\vec{S}_\rho \\
&= \frac{1}{\mu_0}\left(-\oint B_\theta\,dl_\theta\oint E_\phi\,dl_\phi\right) \\
&= -V_\phi(a,t)I_\phi(t)
\end{aligned} \tag{9}$$

The right side represents the rate at which poloidal magnetic energy enters the plasma through the outer boundary. The second term on the left is the resistive dissipation power, which converts electromagnetic energy into kinetic energy of the plasma. Note that this term is not equal to the total Joule heating, $(\vec{E}\cdot\vec{J})$, nor to the component which enters through a parallel Ohm's law, $(E_\parallel J_\parallel)$, except in the large aspect ratio, low beta limit of a tokamak. The first term on the left is primarily the time rate of change of the total magnetic energy content of the plasma plus a term due to changing geometry:

$$\begin{aligned}
\int\frac{\partial}{\partial t}\left(\frac{B_\theta^2}{2\mu_0}\right)dV &= \frac{d}{dt}\int\left(\frac{B_\theta^2}{2\mu_0}\right)dV - \int\left(\frac{B_\theta^2}{2\mu_0}\right)d\dot{V} \\
&= \dot{W}_{B_\theta}(t) - \int\left(\frac{B_\theta^2}{2\mu_0}\right)d\dot{V}
\end{aligned} \tag{10}$$

Solving for the toroidal loop voltage and then integrating over time leads to the Poynting or magnetic energy form of the volt-second balance:

$$\int V_\phi(a,t)\,dt = \int\frac{dt}{I_\phi(t)}\left[\dot{W}_{B_\theta}(t) + \int E_\phi J_\phi\,dV - \int\left(\frac{B_\theta^2}{2\mu_0}\right)d\dot{V}\right] \tag{11}$$

Ignoring the last term gives [2]

$$\Psi_a^P(t) \equiv \int V_\phi(a,t)\,dt \approx \int \frac{dt}{I_\phi(t)}\left[\dot{W}_{B_\theta}(t) + \int E_\phi J_\phi\,dV\right] \tag{12}$$

An alternative form is obtained by defining an internal inductance, $L_{\rm int}^P$ (where the superscript P refers to Poynting's theorem), or inductivity, ℓ_i,

$$L_{\rm int}^P(t) \equiv \frac{\mu_0 R_0 \ell_i(t)}{2} \equiv \frac{2W_{B_\theta}(t)}{I_\phi^2(t)} \tag{13}$$

and an effective resistivity,

$$\mathcal{R}_{\rm eff}(t) \equiv \frac{1}{I_\phi^2(t)}\int E_\phi J_\phi\,dV \tag{14}$$

so that

$$\Psi_a^P(t) = \int dt\left[L_{\rm int}^P(t)\dot{I}_\phi(t) + \frac{1}{2}\dot{L}_{\rm int}^P(t)I_\phi(t) + I_\phi(t)\mathcal{R}_{\rm eff}(t)\right] \tag{15}$$

Although all terms in Eq. (15) have units of magnetic flux, they are in reality quantities defined from the magnetic energy balance. Ejima et al. [2] call the first two terms the inductive component of the flux,

$$\Psi_{\rm ind}^P(t) \equiv \int dt\left[L_{\rm int}^P(t)\dot{I}_\phi(t) + \frac{1}{2}\dot{L}_{\rm int}^P(t)I_\phi(t)\right] \tag{16}$$

This inductive flux does not usually vanish when integrated over an entire pulse since it depends on the time history of the current and its distribution.

Another alternative is to define an effective internal flux linked to the external circuit,

$$\Psi_{\rm int}^P(t) \equiv L_{\rm int}^P(t)I_\phi(t) \tag{17}$$

and express the balance as

$$\Psi_a^P(t) = \int dt\left[\dot{\Psi}_{\rm int}^P(t) - \frac{1}{2}I_\phi(t)\dot{L}_{\rm int}^P(t) + I_\phi(t)\mathcal{R}_{\rm eff}(t)\right] \tag{18}$$

so that the last two terms combined can be called the flux dissipated in establishing the poloidal magnetic energy content of the plasma. Ψ_{int}^P is positive definite and vanishes with the current at the end of a pulse.

In experimental analyses, the time integral of the loop voltage is measured, and the relative assignment of inductive and resistive contributions depends on whether the axial model, Eq. (7), or the Poynting model, Eq. (15) or (18), is used. The internal flux for the axial model, $\Psi_{\rm int}^F$, must be obtained from an MHD equilibrium, while the inductive flux, $\Psi_{\rm ind}^P$, can be determined more directly through magnetic measurements for the Poynting model [2]. The linked and inductive fluxes are always less than the internal flux. Since the remaining flux is labelled the resistive loss, the Poynting model then always indicates a larger resistive loss than the axial model. Care must be taken in predictive analyses not to confuse the various definitions, keeping the proper definition of the resistive loss with the corresponding definition of the inductive term.

4 FLUX AND ENERGY EFFECTS OF MHD ACTIVITY

The plasma particle density, temperature, and current density profiles are modeled in fluid transport codes as a set of coupled diffusion equations with the relevant timescales governed by the particle diffusivity, thermal conductivity, and electrical conductivity, respectively. The evolution of the poloidal flux with respect to the toroidal flux (in the absence of non-ohmically driven currents) is given by [5]:

$$\frac{\partial \Psi'}{\partial t} = \frac{1}{\mu_0}\frac{\partial}{\partial \rho}\left[\frac{\eta_{\|}\rho}{C_1^2}\frac{\partial}{\partial \rho}\left(\frac{C_1 C_2}{\rho}\Psi'\right)\right] \tag{19}$$

where

$$\begin{aligned} C_1 &\equiv V'\langle R^{-2}\rangle \\ C_2 &\equiv V'\langle R^{-2}(\nabla\rho)^2\rangle \\ \rho^2 &\equiv a^2\frac{\Phi}{\Phi_a} \end{aligned} \tag{20}$$

the prime denotes differentiation with respect to radial coordinate ρ, V is the plasma volume contained within the flux surface labeled by ρ, Φ_a is the total toroidal flux in the plasma, and the angle brackets $\langle\,\rangle$ designate a flux surface averaged quantity.

Internal MHD instabilities, on the other hand, occur on an Alfvén timescale and result in a restructuring of the magnetic geometry and profiles. The large disparity between diffusion and Alfvén timescales, $\tau_{\rm diff}/\tau_A \approx 10^5 - 10^{10}$, requires that internal MHD activity be modeled as periodic step changes in plasma geometry and profiles [6], with the redistribution usually based on some variation of Kadomtsev's model [7].

Although the details of when to trigger an internal disruption and of how to reconstruct profiles differ among various transport simulation codes [8,9], a few basic global conservation principles must be observed. If the disruption does not extend to the plasma boundary (i.e., as in an internal disruption), then the layer of undisturbed plasma, which responds on the $\tau_{\rm diff}$ timescale, insulates the effect of the disruption from the exterior system. This leads to conservation of the total number of particles and the total energy content (kinetic plus magnetic) in the disruption region, constraints which are usually obeyed in transport modeling of sawtooth effects. Conservation principles can also be developed for evaluating volt-second consumption.

Reconstructing the poloidal magnetic field after a sawtooth disruption usually starts with an empirical model relating the initial and final helical flux profiles, as in the Kadomtsev model. Then $\vec{B}_\theta$, $\Psi^F_{\rm int}(\rho)$, $I_\phi(\rho)$, $q(\rho)$, h_i, ℓ_i, and $W_{B_\theta}(\rho)$, where ρ is a flux surface label, are all determined from the helical flux and the assumption that the dominant toroidal flux is unperturbed. This assumes that there is no conversion of poloidal flux to toroidal flux during reconnection, but this assumption does not affect the net results. Any conversion to toroidal flux would result in resistive dissipation through a poloidal electric field, since in a quasi-steady-state operating mode there can be no net accumulation or depletion of the toroidal flux. Since the fields are frozen into the outer plasma on the reconnection timescale, the enclosed toroidal current, safety factor, and poloidal field profiles remain unchanged in that region.

Assume that the initial and final poloidal fields, $\vec{B}_{\theta i}$ and $\vec{B}_{\theta f}$, respectively, are known from some model; then carry this change in the poloidal field through the volt-second analyses. Model the step change in the poloidal field around the time of the disruption,

$t = t_d$, by

$$\vec{B}_\theta(\mathbf{x}, t) = \vec{B}_{\theta i}(\vec{x}) H(t_d - t) + \vec{B}_{\theta f}(\vec{x}) H(t - t_d) \tag{21}$$

where H is the Heaviside step function. The internal flux is then

$$\begin{aligned}
\Psi^F_{\text{int}}(t) &= \int \vec{B} \cdot d\vec{S}_\theta \\
&= H(t_d - t) \int \vec{B}_{\theta i} \cdot d\vec{S}_\theta + H(t - t_d) \int \vec{B}_{\theta f} \cdot d\vec{S}_\theta \\
&= \Psi^F_{\text{int},i} + H(t - t_d) \left[\Psi^F_{\text{int},f} - \Psi^F_{\text{int},i} \right] \\
&= \Psi^F_{\text{int},i} + H(t - t_d) \Delta \Psi^F_{\text{int},d}
\end{aligned} \tag{22}$$

where $H(t_d - t) = 1 - H(t - t_d)$ has been used. The sawtooth disruption increases $q(0)$ to a value above unity, and if the total toroidal plasma current and toroidal flux are held constant, this means the current profile is broadened and the change in the internal poloidal flux produced by the sawtooth, $\Delta \Psi^F_{\text{int},d}$, is negative. Substituting Eq. (22) into Eq. (5) and requiring the quantity in brackets to vanish (since the external system cannot respond on the Alfvén timescale to an internal mode) gives

$$V_{\phi d}(0, t) = -\delta(t - t_d) \Delta \Psi^F_{\text{int},d} \tag{23}$$

In other words, the rapid change in the magnetic field must be accompanied by a voltage spike (dictated by Faraday's law). A portion of the internal flux is dissipated by this voltage spike. The loop voltage on axis between disruptions is evaluated from Ohm's law so the total axial loop voltage is

$$V_\phi(0, t) = 2\pi R_{\text{ax}} \eta_\parallel(0, t) J_\phi(0, t) - \sum_d \delta(t - t_d) \Delta \Psi^F_{\text{int},d} \tag{24}$$

where R_{ax} is the major radius of the magnetic axis. The disruption term may also be viewed as the contribution necessary to ensure that $\nabla \times \vec{E}$ in Faraday's law vanishes when integrated over a sawtooth period.

Finally, the axial volt-second balance becomes

$$\begin{aligned}
\Psi^F_a(t) &= \int 2\pi R_{\text{ax}} \eta_\parallel(0, t) J_\phi(0, t)\, dt - \sum_d \Delta \Psi^F_{\text{int},d} + \Psi^F_{\text{int}}(t) \\
&= \Psi^F_R(t) + \Psi^F_d(t) + \Psi^F_{\text{int}}(t),
\end{aligned} \tag{25}$$

where $J_\parallel(0, t) = J_\phi(0, t)$ has been used.

The poloidal magnetic energy around the time of the disruption is given by

$$W_{B_\theta}(t) = W_{B_\theta i} H(t_d - t) + W_{B_\theta f} H(t - t_d) \tag{26}$$

The poloidal magnetic energy is converted to plasma kinetic energy through a spike in the toroidal electric field and current in the disruption region, as seen by balancing the terms inside the brackets in Eq. (12):

$$\begin{aligned}
\dot{W}_{B_\theta}(t) &= (W_{B_\theta f} - W_{B_\theta i}) \delta(t - t_d) \\
&= \Delta W_{B_\theta d} \delta(t - t_d) \\
&= -\int (E_\phi J_\phi)_d \, dV
\end{aligned} \tag{27}$$

The contribution to the volt-second balance from a series of internal disruptions is

$$\Psi_d^P(t) = -\sum_d \frac{\Delta W_{B_\theta d}}{I_\phi} \tag{28}$$

giving the total Poynting volt-second balance of

$$\Psi_a^P(t) = \Psi_R^P(t) + \Psi_d^P(t) + \Psi_{\rm int}^P(t) \tag{29}$$

where the resistive dissipation portion is the integral over the resistive diffusion terms in Eq. (18) between sawteeth:

$$\Psi_R^P(t) = \int dt \left[-\frac{1}{2} I_\phi(t) \dot{L}_{\rm int}^P(t) + I_\phi(t) \mathcal{R}_{\rm eff}(t) \right] \tag{30}$$

5 KADOMTSEV'S MODEL FOR FLUX REDISTRIBUTION

The primary element in the Kadomtsev model for magnetic flux redistribution due to sawtooth activity is the relationship it provides between the initial and final poloidal flux profiles. This relationship is determined by constructing an initial helical flux function associated with $q = 1$, then establishing a final helical flux function that conserves helical flux and monotonically increases with the plasma minor radius.

The toroidal and poloidal fluxes are related through the safety factor by

$$q \equiv \frac{d\Phi}{d\Psi} \tag{31}$$

The poloidal flux is related to the safety factor by

$$\Psi'(\rho) = \frac{2\Phi_a}{a^2} \frac{\rho}{q(\rho)} \tag{32}$$

where ρ is defined in Eq. (20). A helical flux function, Ψ^*, can be defined as the difference between the poloidal flux and the poloidal flux associated with $q = 1$,

$$\begin{aligned} \Psi^*(\rho) &\equiv \Psi(\rho) - \Psi(\rho)\Big|_{q=1} \\ &= \frac{2\Phi_a}{a^2} \int_0^a \left[\frac{1}{q(\rho)} - 1 \right] \rho \, d\rho \end{aligned} \tag{33}$$

If $q < 1$ in some region, then Ψ^* becomes nonmonotonic, a necessary but not sufficient condition for the sawtooth to occur. A sufficient condition is usually specified in terms of the sawtooth period or a critical $q_c < 1$. The relationship between the initial and the final Ψ^* is given by Kadomtsev as

$$\frac{d\Psi_f^*(\rho)}{d\rho} d\rho = \frac{d\Psi_i^*(\rho)}{d\rho}\Big|_{\rho_1} d\rho_1 = \frac{d\Psi_i^*(\rho)}{d\rho}\Big|_{\rho_2} d\rho_2 \tag{34}$$

where the differentials $d\rho$, $d\rho_1$, and $d\rho_2$ are identified with the helical flux elements $d\Psi^* = d\Psi_f^*(\rho) = d\Psi_i^*(\rho_1) = d\Psi_i^*(\rho_2)$ about $\Psi_f^*(\rho) = \Psi_i^*(\rho_1) = \Psi_i^*(\rho_2)$, as illustrated in Fig.1. When $q(0) < 1$ and monotonically increases to $q(a) > 1$, then Ψ_i^* has a maximum at the

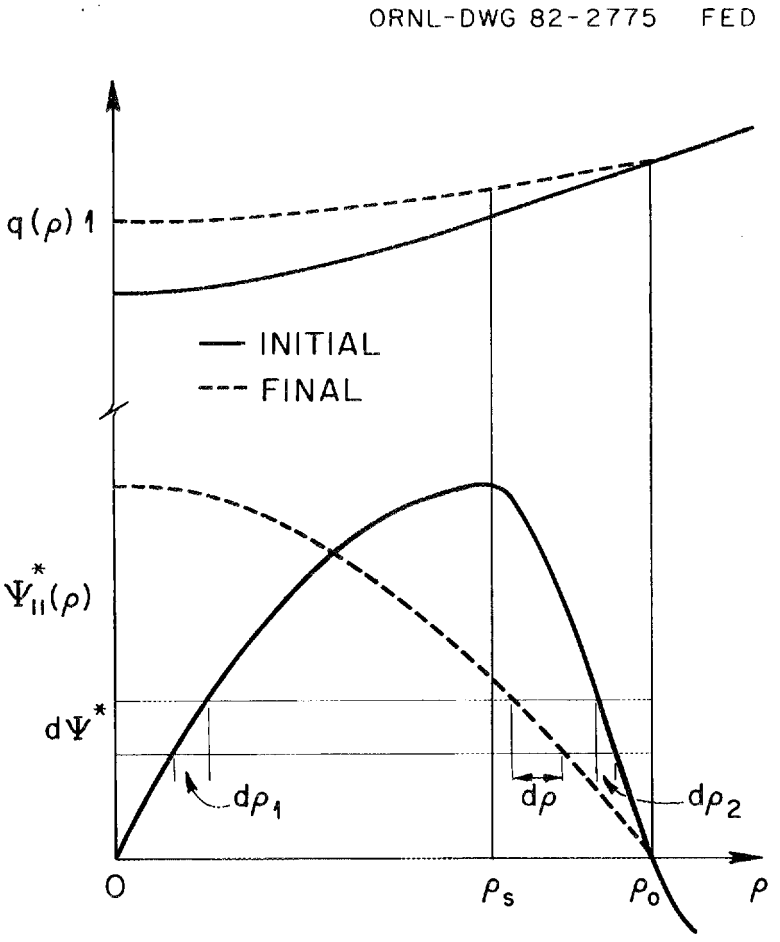

Figure 1: Reconstruction of the helical flux function following the Kadomtsev treatment. The 11 subscript on Ψ^*_{11} designates $(m, n) = (1, 1)$ where $q = m/n$.

$q = 1$ singular surface designated ρ_s. The extent of the reconnection is determined by the range over which Ψ_i^* is multivalued and designated ρ_0. The new poloidal flux is then given by

$$\Psi_f(\rho) = \Psi_f^*(\rho) + \Psi(\rho)\Big|_{q=1} \tag{35}$$

The model has also been generalized to include multiple $q = 1$ surfaces and conditions where $q(0) > 1$ but falls below unity over a finite region away from the axis with full reconnection [10] and with partial reconnection as an explanation of double sawteeth [9].

6 APPLICATION TO CIT

A reexamination of sawtooth activity—confinement and stability effects and possible means of control—has been a major physics issue for CIT [11]. The Kadomtsev-type sawtooth models widely used in transport codes generally predict pronounced central temperature and density fluctuations in low aspect ratio, low-q, shaped plasmas, which include those in CIT. Pressure and shear profiles following a sawtooth may reduce MHD stability limits. In a D-T plasma, the sawtooth crash leads to a reduction in the fusion rate and thus makes ignition more difficult even if global energy confinement is not degraded by sawtooth activity. The applicability of the Kadomtsev and other sawtooth models to CIT and existing experiments is therefore being carefully examined.

The basic machine parameters for CIT are: major radius to the geometric center of the plasma $R_0 = 1.324\,\mathrm{m}$, minor radius in the midplane $a = 0.427\,\mathrm{m}$, elongation $\kappa = 2.0$, triangularity $\delta = 0.41$, vacuum toroidal field $B_{\phi 0} = 10.4\,\mathrm{T}$ at R_0, and toroidal current $I_\phi = 10\,\mathrm{MA}$. The toroidal field and current are ramped simultaneously to minimize the total startup time while eliminating skin current effects (Fig.2). The feasibility of this type of startup scheme has been recently shown by experiments on Alcator C [12]. Ramp rates are dictated by power supply limitations. The flat-top portion at the maximum field parameters shown here is 3.5 s and is limited by Ohmic heating in the toroidal field coils.

The following analysis of the poloidal flux evolution was modeled with the WHIST transport code [13], which evolves the plasma geometry through a series of MHD equilibria generated by the VMOMS code [14]. A sawtooth crash is triggered when $q(0)$ drops below 0.95. The confinement model includes Kaye-Goldston L-mode losses for electrons [15] and Chang-Hinton losses for ions [16]. The parallel electrical resistivity includes neoclassical effects as formulated by Hirshman et al. [17], and $Z_{\mathrm{eff}} \approx 1.5$ is modeled with carbon as the impurity.

The density is ramped concurrently with the toroidal field and current such that the empirical limit on density in ohmically heated plasmas is obeyed. Equal global concentrations of deuterium and tritium are maintained by gas puffing in these simulations to isolate the changes in flux induced by sawtooth activity from the transient effects induced by pellet injection.

Figure 3 shows the effect of sawtooth activity on the plasma density and temperature for an Ohmic CIT case. The effect on the central and line-averaged densities is relatively small. Sawtooth activity does not influence the volume-averaged density because the global particle content is conserved during a sawtooth crash. The electron and ion temperatures are tightly coupled by the high plasma density and thus exhibit the same evolution characteristics. The particle-weighted temperatures are proportional to the average thermal energy content and show a jump at each sawtooth (drop in central temperatures) reflecting the conversion of

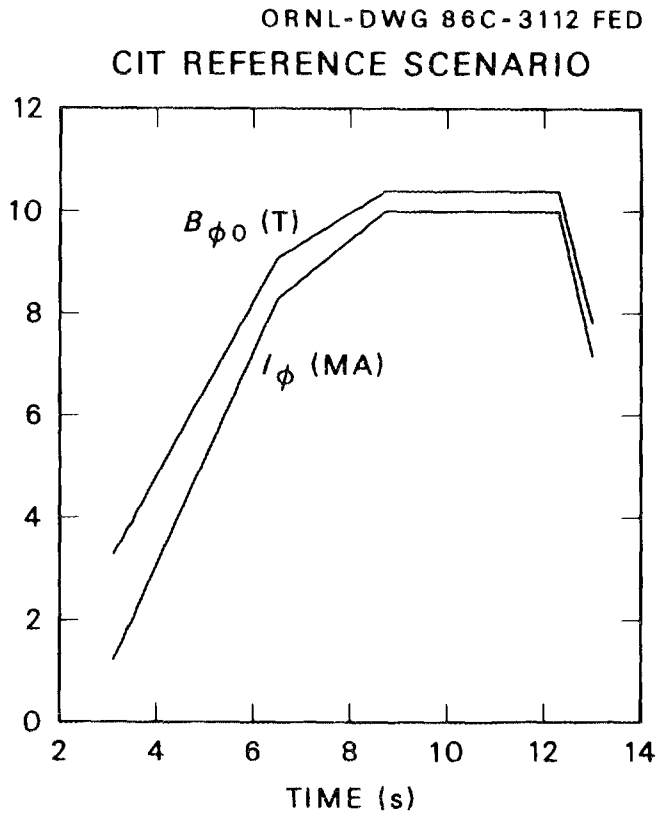

Figure 2: The toroidal field and current are ramped simultaneously. The flat-top portion at the maximum field parameters is 3.5 s.

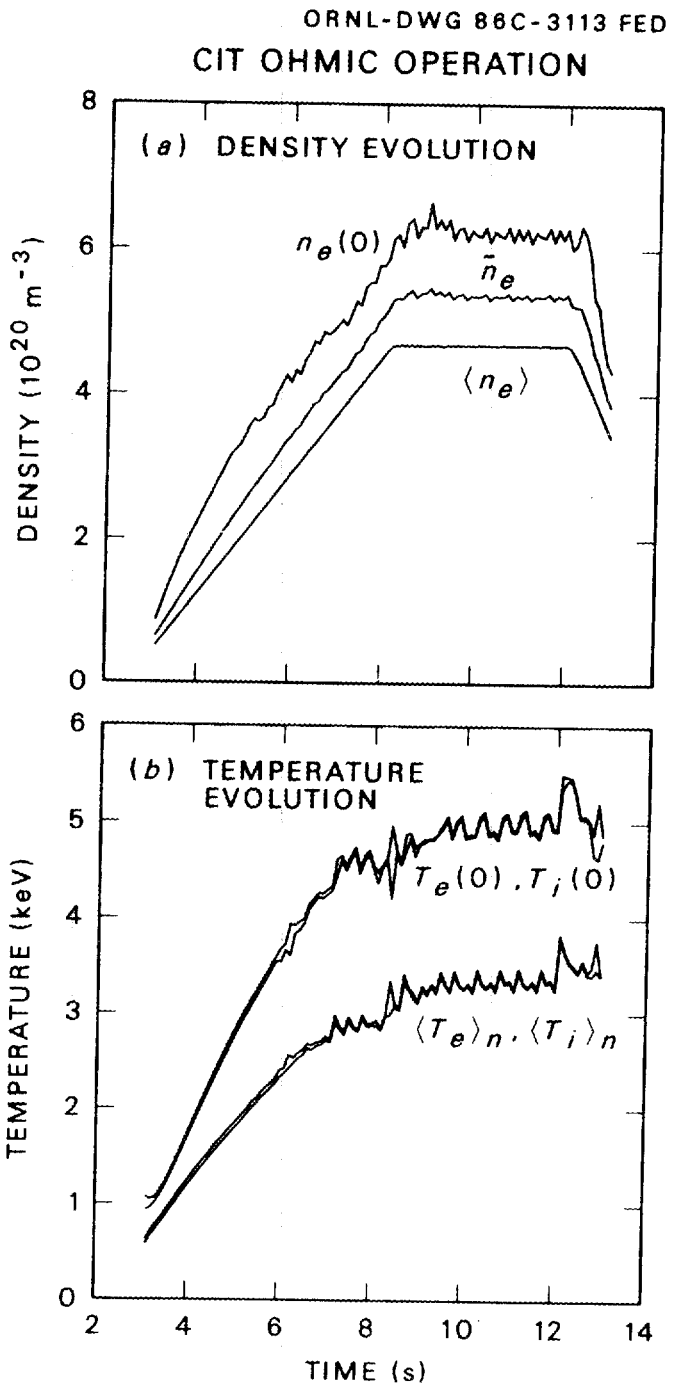

Figure 3: The density is ramped along with the toroidal field and current. (a) Evolution of the central, $n_e(0)$, line-averaged, $\bar{n}_e$, and volume-averaged, $\langle n_e \rangle$, electron densities and (b) evolution of the central, $T(0)$, and particle-weighted, $\langle T \rangle_n$, electron and ion temperatures are shown for the reference Ohmic CIT case.

magnetic to kinetic energy. These jumps are followed by a decay in the plasma kinetic energy content associated with the propagation of a heat pulse from the edge of the disruption zone to the plasma boundary.

According to the Faraday flux balance, the change in internal flux is about 75% of the volt-seconds during the initial fast ramp of the startup phase, with the remainder coming from the axial resistive loss [Fig.4(a)]. After that, sawtooth activity limits the rise in internal flux. By the end of the flat-top phase, volt-second consumption by the sawtooth activity exceeds the resistive loss. With the Poynting method, the change in internal flux consumes only about 40% of the volt-seconds during the fast ramp, and sawtooth activity never makes a very large contribution [Fig. 4(b)]. The total flux consumption in the Poynting method has been set equal to that for the Faraday balance, and the resistive component is then evaluated from

$$\Psi_R^P = \Psi_a^F - \Psi_{\rm int}^P - \Psi_d^P$$

This is easier than evaluating the effective resistance of Eq. (14), which has an implicit coupling of toroidal and poloidal flux changes. This typically differs by as much as 20% from a resistance defined by the parallel Ohmic heating, $E_\| J_\|$, in CIT cases.

The internal inductivity defined from the poloidal magnetic energy content, ℓ_i, is about 60% of that defined from the poloidal flux, h_i, as shown in Fig.5(a). Both are maintained nearly constant through the startup phase and saturate early in the flat-top phase because of sawtooth activity.

The resistive portion of the axial voltage is nearly constant, while both the loop voltage and rate of change in the internal flux exhibit voltage spikes, as shown in Fig. 5(b), for the Faraday flux balance. The data points for the fluxes are at 100 ms intervals (although the time-integrated values in the simulations are obtained on a much finer time mesh), and so the voltage spikes represent values averaged over a 100 ms time interval. The voltage spikes do not result solely from the sawtooth activity—much of the apparent activity comes from the way in which the MHD equilibrium is updated at discrete times (see Ref. [5] for a discussion of various means of coupling MHD equilibrium evolution with transport equations). At each update of the MHD equilibrium, the toroidal current, vacuum toroidal flux, and plasma boundary are fixed in the VMOMS code, and thus small changes in both the poloidal and toroidal fluxes are introduced by a new equilibrium. When the equilibrium geometry is frozen at its initial value and the vacuum toroidal flux is modified continuously, nearly the same flux balance is obtained [Fig.6(a)], and the sawtooth effects on the voltage are more clearly defined [Fig. 6(b)]. The changes in internal flux from sawtooth activity are balanced by increments in the sawtooth dissipation term (not shown) so that the loop voltage remains nearly constant. The MHD equilibrium-induced fluctuations primarily arise from the fact that the calculations are done at random times relative to the sawtooth activity and give negligible net contributions to the flux balance. Under experimental conditions where the plasma boundary is free to move and positional and current feedback have finite response times, details of the voltage response may differ, but poloidal flux contributions should not be significantly different from the results shown here.

If sawtooth activity is turned off altogether by allowing $q(0)$ to drop well below unity, there is a slight increase in the total volt-second consumption (Fig.7); The internal inductivities continue to increase through the pulse when not limited by sawtooth activity.

the internal flux continues to increase throughout the simulation due to a shrinking current channel, so that internal flux consumption in both the axial and Poynting methods is much greater than the case where $q(0)$ is limited to about unity by sawtoothing. This is

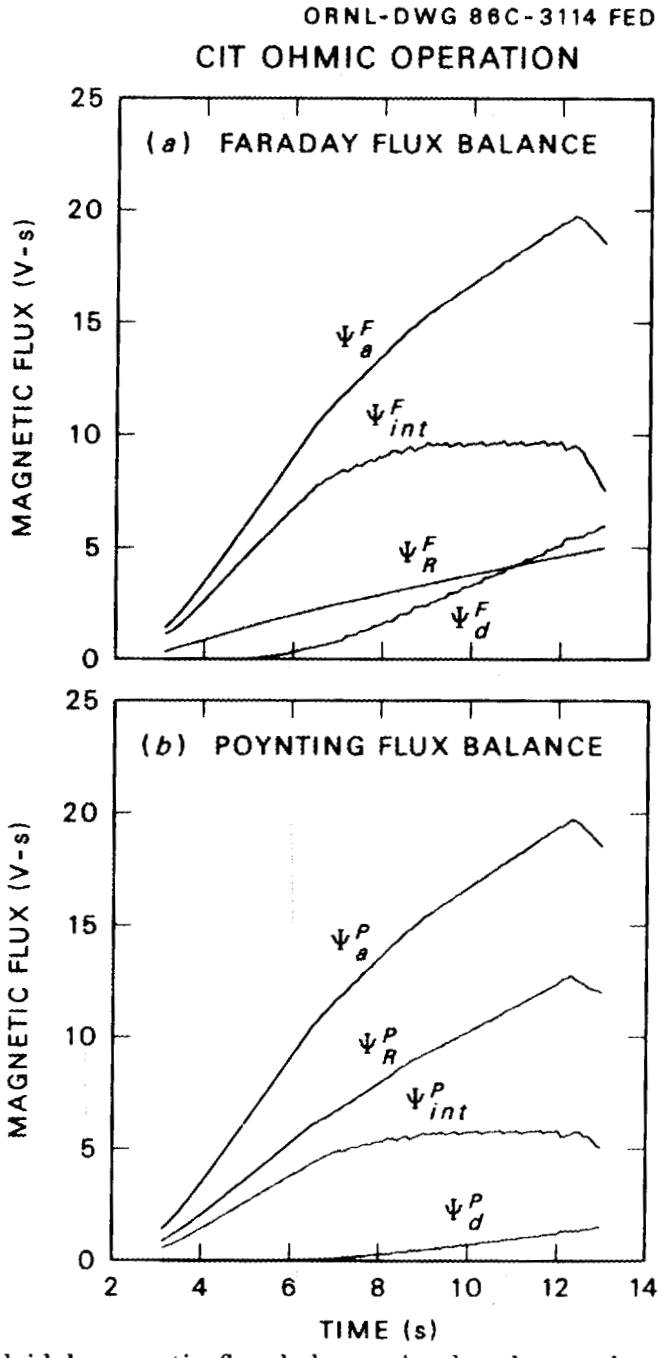

Figure 4: The poloidal magnetic flux balances in the plasma show the time-integrated loop voltage, Ψ_a, the internal component, $\Psi_{\rm int}$, the resistive loss, Ψ_R, and the sawtooth disruption loss, Ψ_d, as determined by (a) Faraday's law and (b) the Poynting equation for the reference Ohmic CIT case.

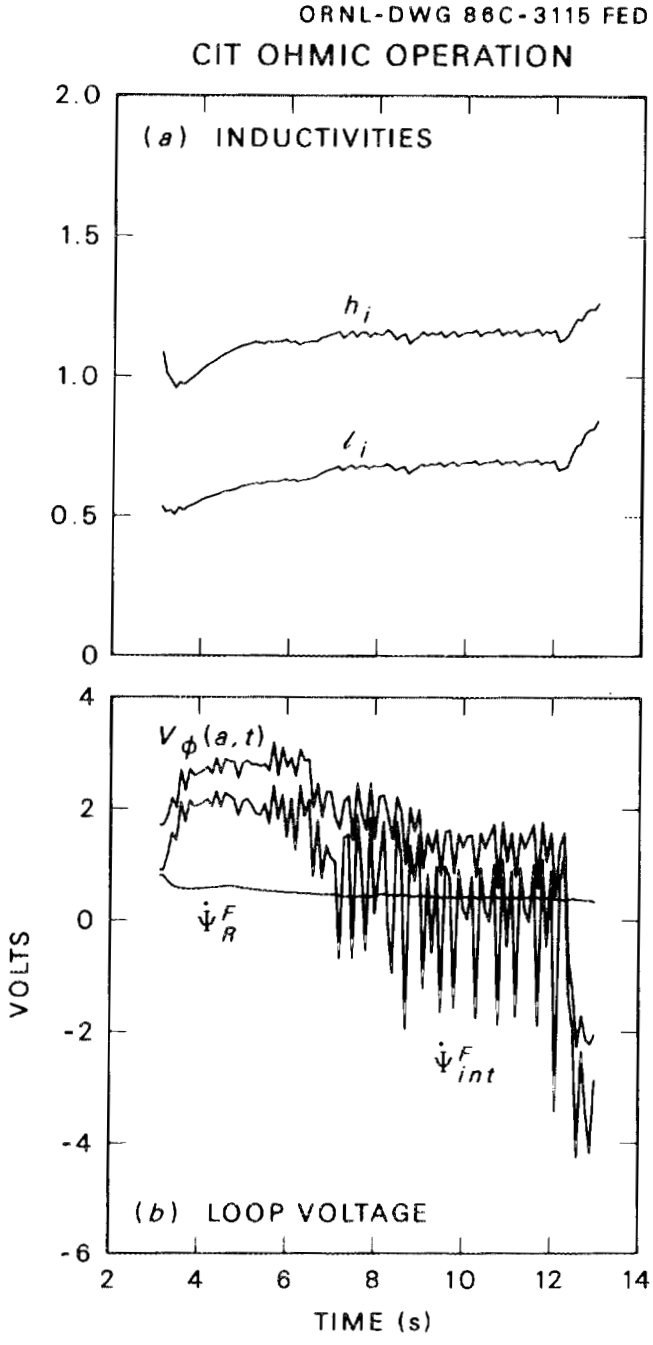

Figure 5: The evolution of (a) the internal inductivites defined from the poloidal magnetic flux, h_i, and poloidal magnetic energy, ℓ_i, and (b) the toroidal loop voltage, V_ϕ, with contributions from the resistive (axial voltage) term, $\dot{\Psi}^F_R$, and the change in internal flux, $\dot{\Psi}^F_{\rm int}$, for the reference Ohmic CIT case.

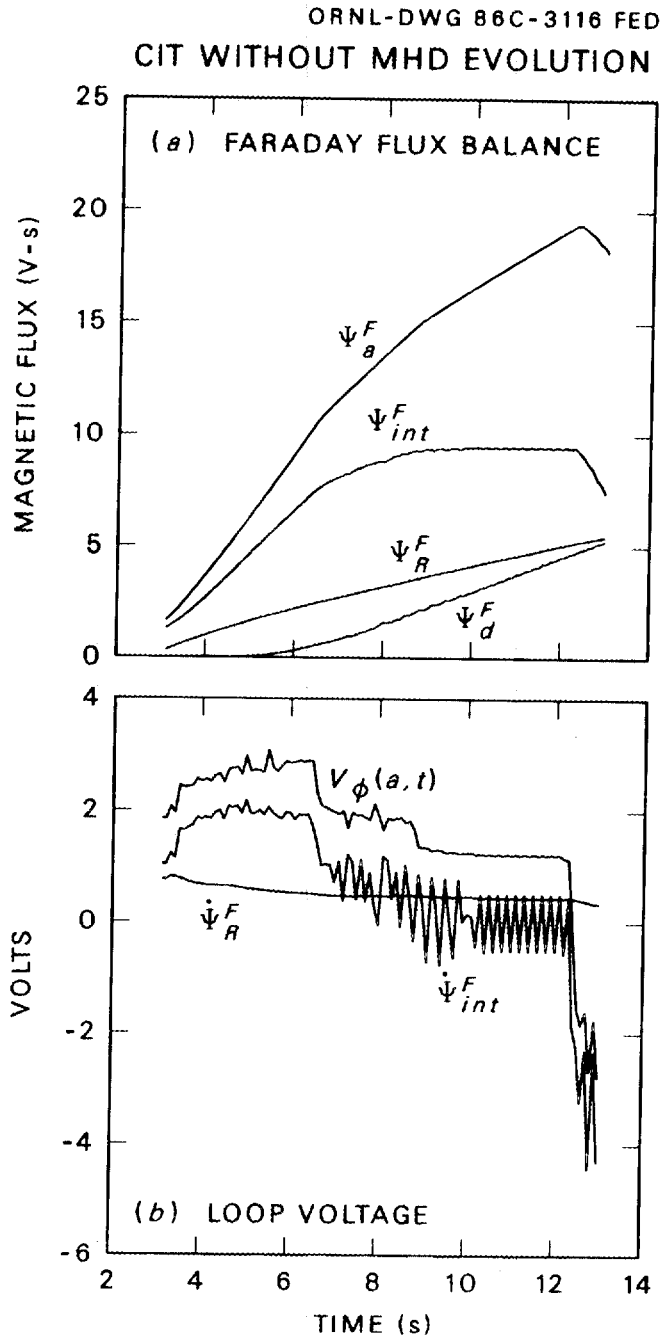

Figure 6: The evolution of (a) the poloidal flux and its components and (b) the loop voltage and its components, as determined by Faraday's law for the reference Ohmic CIT case with the stepwise evolution of the MHD equilibrium removed.

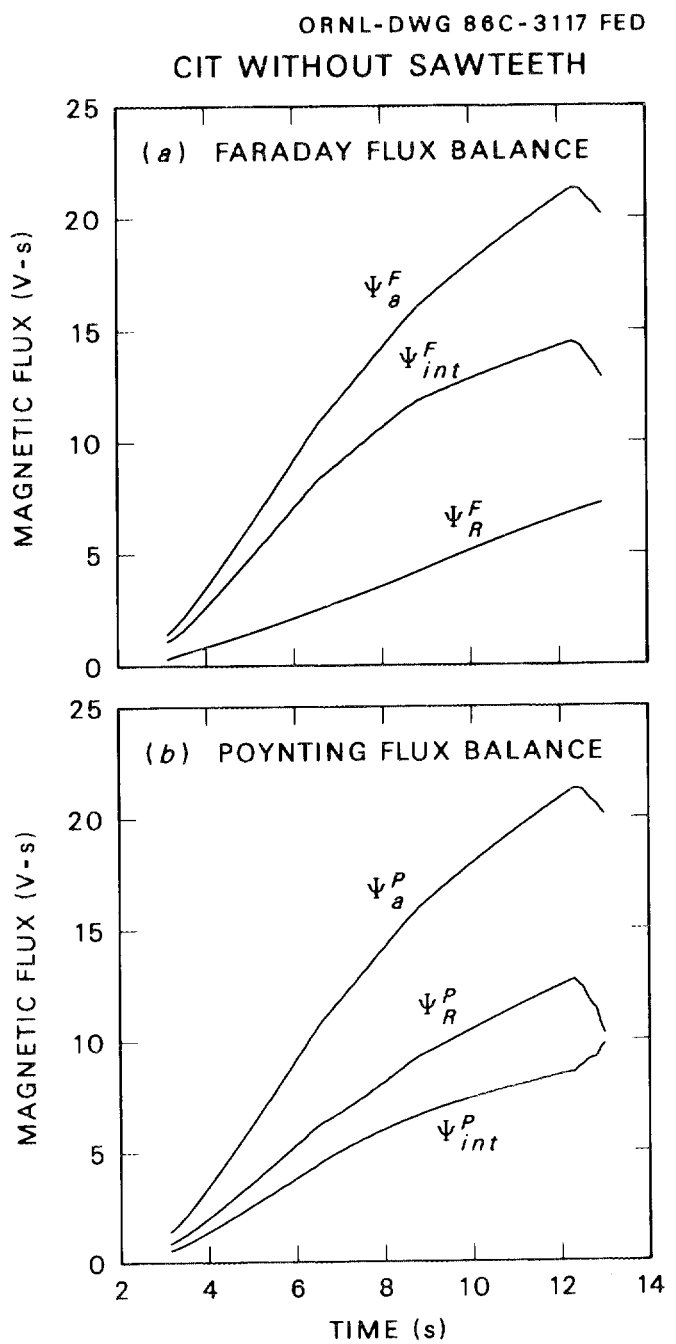

Figure 7: The evolution of the poloidal flux and its components as determined by (a) Faraday's law and (b) the Poynting equation for the reference Ohmic CIT case with sawtooth activity removed.

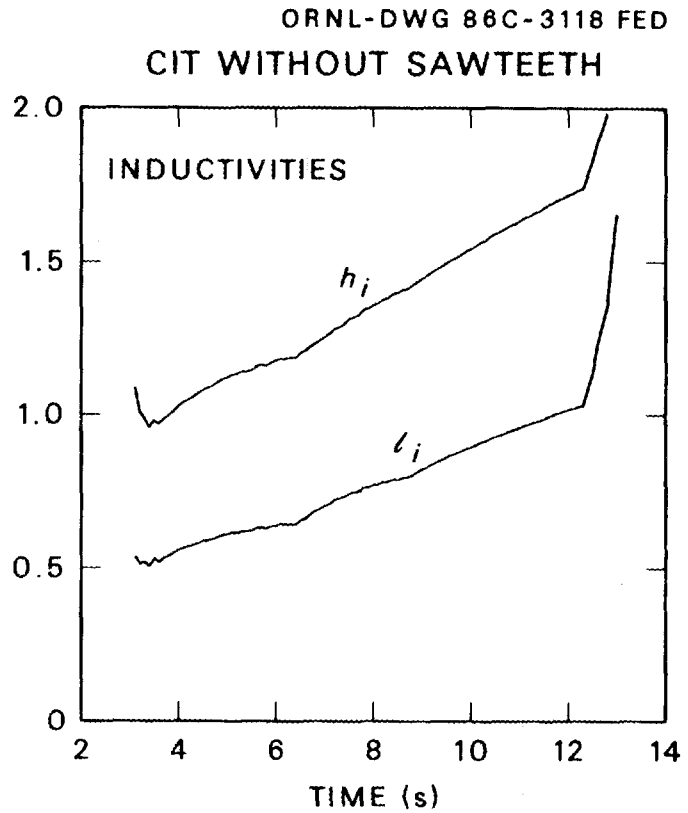

Figure 8: The internal inductivities continue to increase through the pulse when not limited by sawtooth activity.

illustrated by the increasing inductivities (Fig. 8). Ψ_R^F is also greater in the non-sawtoothing case because of its sensitivity to axial current density. As the voltage is swung negative to shut down the plasma, a large negative skin current is introduced at the plasma edge and the inductivities climb rapidly. Under these conditions the plasma would probably be disruptive.

In an ignited plasma the volt-second consumption is reduced because of the lower plasma resistivity. An ignited CIT case is shown in Figs. 9 and 10 where 15 MW of off-axis ICRH heating is applied in the interval $t = 6.5-8.5$ s. The longer resistive timescale causes the q-profile to become less rigid, introducing more variety in the sawtooth reconnection region, a somewhat longer period, and larger density and temperature fluctuations (Fig. 9). The sawtooth contribution to poloidal flux balance is reduced by either method of accounting (Fig. 10), even though the thermal fluctuations are much larger.

7 SUMMARY

When sawtooth activity is invoked as a means of constraining the current density and q-profiles, the consequences of the constraint can be incorporated in the poloidal flux balance, whether Faraday's law or the poloidal component of the Poynting equation is used. For discrete sawtooth models, such as the Kadomtsev model used here, conservation principles can be used to evaluate the net flux changes. Similar results can be obtained by continual enhancement of the parallel resistivity in the sawtooth region, analogous to the way particle

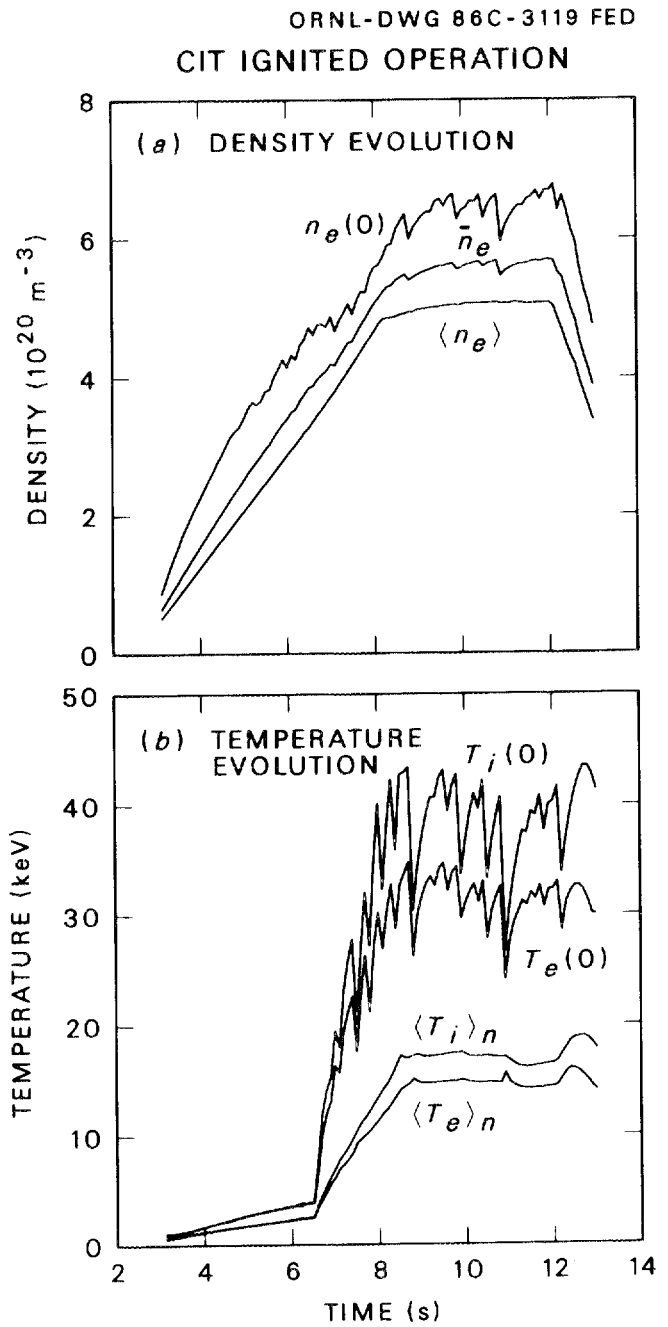

Figure 9: Evolution of (a) the central, line-averaged, and volume-averaged electron densities and (b) the central and particle-weighted electron and ion temperatures for an ignited CIT case.

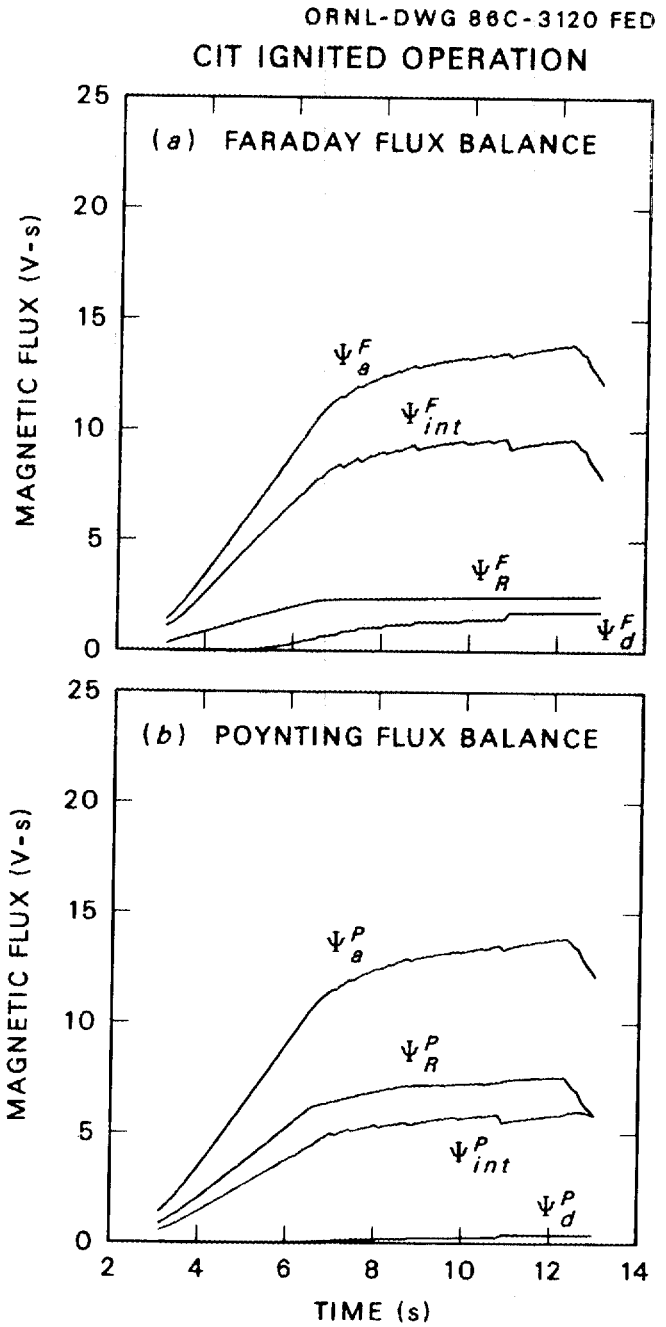

Figure 10: The evolution of the poloidal flux and its components as determined by (a) Faraday's law and (b) the Poynting equation for the ignited CIT case.

and thermal diffusivities are enhanced to simulate the effects of sawteeth. In any case, care must be taken to self-consistently evaluate the various terms from either Faraday's law or the Poynting equation because the relative contributions can vary widely even if the totals are the same. Sawtooth activity can represent a significant portion of the flux consumption in Faraday's law, which highlights the axial voltage, while it is a much smaller term in the Poynting balance, which follows changes in the poloidal magnetic energy content.

The disruptive term in the Faraday flux balance can be checked experimentally through evaluation of the remaining terms of Eq. (25); the left side is the measured loop voltage minus the external flux, the axial loss can be inferred from Spitzer resistivity and a current density corresponding to $q(0) \approx 1$, and the internal flux can be determined from MHD equilibrium analysis. Errors are minimized if this analysis is applied to a long flat-top phase at low $q(a)$.

The Kadomtsev model for sawtooth activity has been challenged recently because a variety of detailed observations on many experiments do not fit the expectations of the model. These observations include shorter than expected crash times, the occasional lack of precursor oscillations and existence of postcursor oscillations, multiple sawteeth, soft X-ray emission profiles showing the growth of a cold bubble rather than an island originating at the $q = 1$ radius, and most notably the possibility that $q(0)$ may be significantly less than unity throughout the sawtooth phase under some conditions in TEXTOR [18]. Theoretical models are being developed that accommodate at least some of these features [19,20], but they have not reached the point where triggering conditions and the relationship between initial and final states can be specified in closed form for use in the type of analysis presented in this paper. This analysis is applicable to any type of discrete MHD activity regardless of the fast timescale details as long as the relationship between initial and final internal flux is known.

REFERENCES

[1] R. J. Hawryluk, K. Bol, and D. Johnson, *Nucl. Fusion* **19**, 1519 (1979).

[2] S. Ejima et al., *Nucl. Fusion* **22**, 1313 (1982).

[3] S. C. Jardin and W. Park, *Phys. Fluids* **24**, 679 (1981).

[4] S. P. Hirshman and G. H. Neilson, *Phys. Fluids* **29**, 790 (1986).

[5] J. Blum and J. Le Foll, *Comput. Phys. Rep.* **1**, 465 (1984).

[6] W. A. Houlberg and J. T. Hogan, *Nucl. Technol./Fusion* **3**, 244 (1983).

[7] B. B. Kadomtsev, *Sov. J. Plasma Phys.* **1**, 389 (1975).

[8] Y. N. Dnestrovskii, S. E. Lysenko, and R. Smith, *Sov. J. Plasma Phys.* **3**, 9 (1977).

[9] W. Pfeiffer, *Nucl. Fusion* **25**, 673 (1985).

[10] V. V. Parail and G. V. Pereversev, *Sov. J. Plasma Phys.* **6**, 14 (1980).

[11] J. Schmidt et al., in *Plasma Physics and Controlled Nuclear Fusion Research (Proc. 11th Int. Conf. Kyoto, 1986)* (International Atomic Energy Agency, Vienna, 1987) [paper H-I-2 in press].

[12] R. R. Parker et al., *Bull. Am. Phys. Soc.* **31**, 1589 (1986).

[13] W. A. Houlberg, S. E. Attenberger, and L. L. Lao, ORNL/TM-8193, Oak Ridge National Lab. (1982).

[14] L. Lao, S. P. Hirshman, and R. M. Wieland, *Phys. Fluids* **24**, 1431 (1981).

[15] S. M. Kaye, *Phys. Fluids* **28**, 2327 (1985).

[16] C. S. Chang and F. L. Hinton, *Phys. Fluids* **25**, 1493 (1982).

[17] S. P. Hirshman, R. J. Hawryluk, and B. Birge, *Nucl. Fusion* **17**, 611 (1977).

[18] H. Soltwisch et al., in *Plasma Physics and Controlled Nuclear Fusion Research (Proc. 11th Int. Conf. Kyoto, 1986)* (International Atomic Energy Agency, Vienna, 1987) [paper A-V-1 in press].

[19] J. A. Wesson, *Comments Plasma Phys. Controlled Fusion* **28**, 243 (1986).

[20] R. E. Denton et al., *Phys. Rev. Lett.* **56**, 2477 (1986).

ORNL/TM-10382
Dist. Category UC-20 g

1. S. E. Attenberger
2. B. A. Carreras
3. R. A. Dory
4. S. P. Hirshman
5. J. T. Hogan
6. H. C. Howe
7. G. H. Neilson
8. Y-K. M. Peng
9. J. Sheffield
10. J. S. Tolliver
11. N. A. Uckan
12. Laboratory Records Department
13. Laboratory Records, ORNL-RC
14. Document Reference Section
15. Central Research Library
16. Fusion Energy Division Library
17–18. Fusion Energy Division Publications Office
19. ORNL Patent Office

EXTERNAL DISTRIBUTION

20. Office of the Assistant Manager for Energy Research and Development, U.S. Department of Energy, Oak Ridge Operations Office, P. O. Box E, Oak Ridge, TN 37831
21. J. D. Callen, Department of Nuclear Engineering, University of Wisconsin, Madison, WI 53706-1687
22. J. F. Clarke, Director Office of Fusion Energy, Office of Energy Research, ER-50 Germantown, U.S. Department of Energy, Washington, DC 20545
23. R. W. Conn, Department of Chemical, Nuclear, and Thermal Engineering, University of California, Los Angeles, CA 90024
24. S. O. Dean, Fusion Power Associates, 2 Professional Drive, Suite 248, Gaithersburg, MD 20879
25. H. K. Forsen, Bechtel Group, Inc., Research Engineering, P. O. Box 3965, San Francisco, CA 94105
26. J. R. Gilleland, GA Technologies, Inc., Fusion and Advanced Technology, P.O. Box 81608, San Diego, CA 92138
27. R. W. Gould, Department of Applied Physics, California Institute of Technology, Pasadena, CA 91125
28. R. A. Gross, Plasma Research Laboratory, Columbia University, New York, NY 10027
29. D. M. Meade, Princeton Plasma Physics Laboratory, P.O. Box 451, Princeton, NJ 08544
30. M. Roberts, International Programs, Office of Fusion Energy, Office of Energy Research, ER-52 Germantown, U.S. Department of Energy, Washington, DC 20545
31. W. M. Stacey, School of Nuclear Engineering and Health Physics, Georgia Institute of Technology, Atlanta, GA 30332
32. D. Steiner, Nuclear Engineering Department, NES Building, Tibbetts Avenue, Rensselaer Polytechnic Institute, Troy, NY 12181
33. R. Varma, Physical Research Laboratory, Navrangpura, Ahmedabad 380009, India

34. Bibliothek, Max-Planck Institut fur Plasmaphysik, D-8046 Garching, Federal Republic of Germany,
35. Bibliothek, Institut fur Plasmaphysik, KFA, Postfach 1913, D-5170 Julich, Federal Republic of Germany,
36. Bibliotheque, Centre de Recherches en Physique des Plasmas, 21 Avenue des Bains, 1007 Lausanne, Switzerland
37. F. Prevot, CEN/Cadarache, Departement de Recherches sur la Fusion Controlee, F-13108 Saint-Paul-lez-Durance Cedex, France
38. Documentation S.I.G.N., Departement de la Physique du Plasma et de la Fusion Controlee, Centre d'Etudes Nucleaires, B.P. 85, Centre du Tri, F-38031 Grenoble, France
39. Library, Culham Laboratory, UKAEA, Abingdon, Oxfordshire, OX14 3DB, England
40. Library, FOM-Instituut voor Plasma-Fysica, Rijnhuizen, Edisonbaan 14, 3439 MN Nieuwegein, The Netherlands
41. Library, Institute of Plasma Physics, Nagoya University, Nagoya 464, Japan
42. Library, International Centre for Theoretical Physics, P.O. Box 586, I-34100 Trieste, Italy
43. Library, Laboratorio Gas Ionizatti, CP 56, I-00044 Frascati, Rome, Italy
44. Library, Plasma Physics Laboratory, Kyoto University, Gokasho, Uji, Kyoto, Japan
45. Plasma Research Laboratory, Australian National University, P.O. Box 4, Canberra, A.C.T. 2000, Australia
46. Thermonuclear Library, Japan Atomic Energy Research Institute, Tokai Establishment, Tokai-mura, Naka-gun, Ibaraki-ken, Japan
47. G. A. Eliseev, I. V. Kurchatov Institute of Atomic Energy, P.O. Box 3402, 123182 Moscow, U.S.S.R.
48. V. A. Glukhikh, Scientific-Research Institute of Electro-Physical Apparatus, 188631 Leningrad, U.S.S.R.
49. I. Shpigel, Institute of General Physics, U.S.S.R. Academy of Sciences, Ulitsa Ulitsa Vavilova 38, Moscow, U.S.S.R.
50. D. D. Ryutov, Institute of Nuclear Physics, Siberian Branch of the Academy of Sciences of the U.S.S.R., Sovetskaya St. 5, 630090 Novosibirsk, U.S.S.R.
51. V. T. Tolok, Kharkov Physical-Technical Institute, Academical St. 1, 310108 Kharkov, U.S.S.R.
52. Library, Academia Sinica, P.O. Box 3908, Beijing, China (PRC)
53. D. Crandall, Experimental Plasma Research Branch, Division of Development and Technology, Office of Fusion Energy, Office of Energy Research, ER-542 Germantown, U.S. Department of Energy, Washington, DC 20545
54. N. A. Davies, Office of the Associate Director, Office of Fusion Energy, Office of Energy Research, ER-51 Germantown, U.S. Department of Energy, Washington, DC 20545
55. D. B. Nelson, Director, Division of Applied Plasma Physics, Office of Fusion Energy, Office of Energy Research, ER-54 Germantown, U.S. Department of Energy, Washington, DC 20545

56. E. Oktay, Division of Confinement Systems, Office of Fusion Energy, Office of Energy Research, ER-55 Germantown, U.S. Department of Energy, Washington, DC 20545

57. W. Sadowski, Fusion Theory and Computer Services Branch, Division of Applied Plasma Physics, Office of Fusion Energy, Office of Energy Research, ER-541 Germantown, U.S. Department of Energy, Washington, DC 20545

58. P. M. Stone, Fusion Systems Design Branch, Division of Development and Technology, Office of Fusion Energy, Office of Energy Research, ER-532 Germantown, U.S. Department of Energy, Washington, DC 20545

59. J. M. Turner, International Programs, Office of Fusion Energy, Office of Energy Research, ER-52 Germantown, U.S. Department of Energy, Washington, DC 20545

60. R. E. Mickens, Atlanta University, Department of Physics, Atlanta, GA 30314

61. M. N. Rosenbluth, RLM 11.218, Institute for Fusion Studies, University of Texas, Austin, TX 78712

62. Duk-In Choi, Department of Physics, Korea Advanced Institute of Science and Technology, P.O. Box 150, Chong Ryang-Ri, Seoul, Korea

63. Theory Department Read File, c/o D. W. Ross, University of Texas, Institute for Fusion Studies, Austin, TX 78712

64. Theory Department Read File, c/o R. C. Davidson, Director, Plasma Fusion Center, NW 16-202, Massachusetts Institute of Technology, Cambridge, MA 02139

65. R. R. Parker, Plasma Fusion Center, NW 16-288, Massachusetts Institute of Technology, Cambrige, MA 02139

66. Theory Department Read File, c/o R. White, Princeton Plasma Physics Laboratory, P.O. Box 451, Princeton, NJ 08544

67. Library of Physics Department, University of Ioannina, Ioannina, Greece

68. Theory Department Read File, c/o L. Kovrizhnykh, Lebedev Institute of Physics, Academy of Sciences, 53 Leninsky Prospect, 117924 Moscow, U.S.S.R.

69. Theory Department Read File, c/o B. B. Kadomtsev, I. V. Kurchatov Institute of Atomic Energy, P.O. Box 3402, 123182 Moscow, U.S.S.R.

70. Theory Department Read File, c/o T. Kamimura, Institute of Plasma Physics, Nagoya University, Nagoya 464, Japan

71. Theory Department Read File, c/o C. Mercier, Departemente de Recherches sur la Fusion Controlee, B.P. No. 6, F-92260 Fontenay-aux-Roses (Seine), France

72. Theory Department Read File, c/o T. E. Stringer, JET Joint Undertaking, Culham Laboratory, Abingdon Oxfordshire, OX14 3DB, England

73. Theory Department Read File, c/o R. Briscoe, Culham Laboratory, Abingdon, Oxfordshire OX14 3DB, England

74. Theory Department Read File, c/o D. Biskamp, Max-Planck-Institut fur Plasmaphysik, D-8046 Garching, Federal Republic of Germany

75. Theory Department Read File, c/o T. Takeda, Japan Atomic Energy Research Institute, Tokai Establishment, Tokai-mura, Naka-gun, Ibaraki-ken, Japan

76. Theory Department Read File, c/o J. Greene, GA Technologies, Inc., P.O. Box 81608, San Diego, CA 92138

77. Theory Department Read File, c/o L. D. Pearlstein, L-630, Lawrence Livermore National Laboratory, P.O. Box 5511, Livermore, CA 94550

78. Theory Department Read File, c/o R. Gerwin, CTR Division, Los Alamos National Laboratory,

    P.O. Box 1663, Los Alamos, NM 87545

79. R. J. Hawryluk, Princeton Plasma Physics Laboratory, P.O. Box 451, Princeton, NJ 08544

80. D. E. Post, Princeton Plasma Physics Laboratory, P.O. Box 451, Princeton, NJ 08544

81. M. G. Bell, Princeton Plasma Physics Laboratory, P.O. Box 451, Princeton, NJ 08544

82. S. C. Jardin, Princeton Plasma Physics Laboratory, P.O. Box 451, Princeton, NJ 08544

83. R. G. Bateman, Princeton Plasma Physics Laboratory, P.O. Box 451, Princeton, NJ 08544

84. C. K. Phillips, Princeton Plasma Physics Laboratory, P.O. Box 451, Princeton, NJ 08544

85. D. R. Mikkelsen, Princeton Plasma Physics Laboratory, P.O. Box 451, Princeton, NJ 08544

86. S. Ejima, GA Technologies, Inc., P.O. Box 85608, San Diego, CA 92138

87. A. G. Kellman, GA Technologies, Inc., P.O. Box 85608, San Diego, CA 92138

88. L. L. Lao, GA Technologies, Inc., P.O. Box 85608, San Diego, CA 92138

89. G. A. Emmert Department of Nuclear Engineering, University of Wisconsin, Madison, WI 53706-1687

90. P. R. Thomas, JET Joint Undertaking, Culham Laboratory, Abingdon, Oxfordshire, OX14 3DB, England

91. M. L. Watkins, JET Joint Undertaking, Culham Laboratory, Abingdon, Oxfordshire, OX14 3DB, England

92–212. Given distribution according to TIC-4500, Magnetic Fusion Energy (Category Distribution UC-20g, Theoretical Plasma Physics)